Available online at www.sciencedirect.com

SciVerse ScienceDirect

Ceramics International 38 (2012) 4661–4667

CERAMICS INTERNATIONAL

www.elsevier.com/locate/ceramint

The fracture toughness of alumina coatings plasma-sprayed at different in situ temperatures

Ya-Zhe Xing [a,*], Qiu-Lan Wei [b], Jian-Min Hao [a]

[a] School of Materials Science and Engineering, Chang'an University, Xi'an, Shaanxi 710064, China
[b] Department of Automotive Engineering, Shaanxi College of Communication Technology, Xi'an, Shaanxi 710018, China

Received 27 June 2011; received in revised form 2 February 2012; accepted 9 February 2012
Available online 21 February 2012

Abstract

Alumina coatings were prepared by atmospheric plasma spraying through controlling the surface temperature of the coatings during spraying. Both the polished and fractured cross-section microstructures of the coatings were characterized by scanning electron microscopy (SEM). The phase structures of the coatings and the feedstock were analyzed by X-ray diffraction technique (XRD). The microstructure and phase structure of the coatings prepared at different substrate temperatures were examined. SEM observations show that the intersplat bonding within the coatings was significantly improved by increasing the substrate temperature. The fracture toughness of the deposits was measured by indentation methods. For the coatings prepared at low substrate temperatures, the fracture toughness increased with the substrate temperature due to the improvement in the intersplat bonding. However, a significant decrease in the fracture toughness was found for the coatings prepared at high substrate temperatures. The change in phase structure of the coatings suggested that the residual tensile stress mainly resulted from phase transformation from γ-alumina to α-alumina at high substrate temperature should answer for the decline in the fracture toughness.

Keywords: Plasma spraying; Alumina; Phase transformation; Fracture toughness

1. Introduction

Traditional plasma sprayed alumina coatings exhibit a lamellar structure, which affects coating properties [1,2]. The previous study revealed that only limited lamellar interface is bonded together in APS ceramic coatings and the maximum bonding ratio between lamellar interfaces is about one-third of the total apparent interfaces [3]. The limited interface bonding dominates thermal and electrical conductivities of the coating [2]. In our previous studies, it was found that the electrical conductivity was significantly increased when YSZ was deposited on a substrate heated to a high temperature compared with that deposited at ambient temperature [4,5]. The improved conductivity is attributed to the improved lamellar interface bonding at high substrate temperature. From the previous investigations [6–10], it can be suggested that increasing substrate temperature may improve the lamellar bonding. Although Heintze and Uematsu [11] obtained α-Al_2O_3 coatings by plasma spraying process through elevating the surface temperature of the coating during deposition, few attempts were made to investigate systematically the effect of the substrate temperature on the fracture toughness of plasma-sprayed alumina coatings.

In this work, during deposition of alumina coatings by plasma spraying, the surface temperature of the coatings was controlled carefully. Alumina coatings were prepared by plasma spraying under different coating surface temperatures (substrate temperature). The variations in the microstructure and the fracture toughness of the coatings were investigated.

2. Experimental

2.1. Material and coating preparation

Commercially available fuse-crushed Al_2O_3 powders were used for coating preparation. The powders have a particle size range from 20 to 50 μm, as shown in Fig. 1. The alumina was deposited on a stainless steel substrate surface by a commercial

* Corresponding author. Tel.: +86 29 82334590; fax: +86 29 82334590.
E-mail address: xingyz@chd.edu.cn (Y.-Z. Xing).

0272-8842/$36.00
doi:10.1016/j.ceramint.2012.02.048

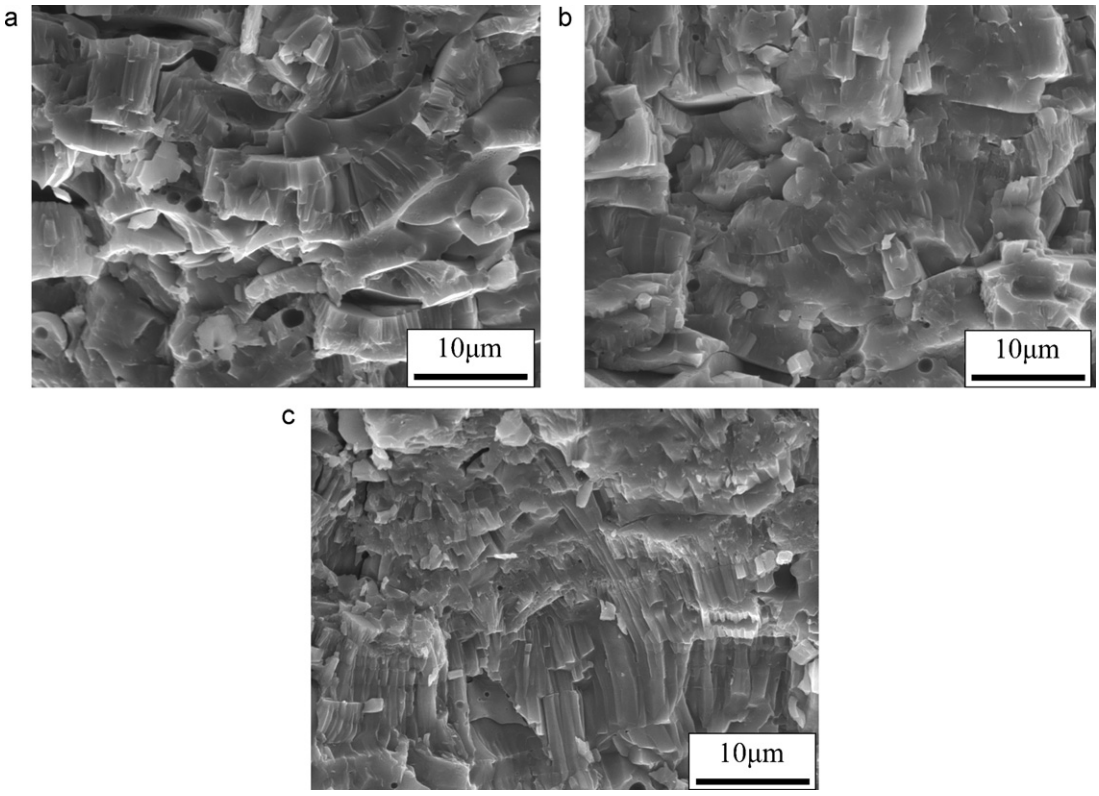

Fig. 1. Fractured cross-sections for (a) C1, (b) C2, and (c) C5 [18].

plasma spray system (80 kW class, Jiujiang Spraying Equipment Factory, China). The plasma torch was operated at 36 kW. The pressures of primary gas Ar and secondary gas H_2 were fixed at 0.7 and 0.4 MPa, respectively. The flow rates of Ar and H_2 were 33 l/min and 2 l/min, respectively. The powder was fed into a plasma jet using an internal powder port. The torch–substrate distance during deposition was 80 mm. A robot was used to drive the plasma torch back and forth across the substrate surface during deposition.

To prepare the samples for the SEM observations of both fractured and polished cross-section, free-standing alumina coatings (about 400 μm in thickness) were obtained through post-spray dissolution of the substrate in hydrochloric acid solution. During deposition, the mean substrate temperature was controlled in the range from 240 to 1120 °C through heating with a flame gun combined the plasma torch from the front of the substrate and cooling with the compressed air from the back of the substrate. A pyrometer (RAYR312ML3U, Raytek, USA) was placed in front of the substrate to monitor the substrate temperature, which was coating surface temperature as the first layer of alumina was deposited. The substrate was heated to the desired temperature by the flame gun in one minute, and then started the spraying process. During spraying, to make the substrate temperature (coating surface temperature) to be identical with the desired temperature as far as possible, both the flame gun–substrate distance and the flow rate of the compressed air were changed at any moment. After spraying, only the flame gun kept working and the flame gun–substrate distance was increased slowly to ensure a slow cooling rate of the coating-substrate system. As the coating surface temperature reached below 150 °C, the flame gun stopped working and the coating-substrate system was cooled to room temperature in the air. The change in the substrate temperature during coating spraying was listed in Table 1.

2.2. Characterization of the alumina coatings

Cross-sections of alumina coatings were carefully polished for microstructure examination. The microstructure of the coatings was characterized by scanning electron microscopy (SEM, VEGA II-XMU, TESCAN, Czech). To examine the columnar structure and lamellar interface bonding, the coatings were fractured in a direction perpendicular to the coating surface. The fractured surface was examined using SEM. The phase structure of the coatings was analyzed by X-ray diffraction (XRD).

Table 1
Substrate temperature during deposition of the coatings.

Sample	Substrate temperature (°C)
C1	240 ± 73
C2	430 ± 82
C3	760 ± 91
C4	960 ± 121
C5	1120 ± 111

2.3. Measurements of the fracture toughness of the alumina coatings

The fracture toughness of the coating cross-section was measured by diamond pyramid (Vickers) indentation test [12]. Vickers' indentation was conducted with diamond indenter (HVS-50Z/LCD, Shanghai Taiming Optical Corporation, China) under a load of 50 kgf for a loading time of 10 s to induce cracking of the alumina coating on the cross section. Ten tests were conducted at the center locations of the coating thickness for each sample. During testing, one diagonal was parallel to the coating surface and the other was perpendicular to the coating surface. Although there are many formulae can be used to calculate the fracture toughness, Niihara [13] and Anstis formulae had been employed to calculate the fracture toughness of thermally sprayed coatings [14–16]. For the plasma-sprayed ceramic coatings, the fracture toughness should be lower than that of bulk materials due to its limited interlamellar bonding [2]. However, the fracture toughness value calculated by Niihara formula for C1 was higher than that of bulk alumina. Therefore, in present work, the indentation fracture toughness was calculated using the Anstis formula [12]:

$$K_{1C} = 0.016\left(\frac{E}{H}\right)^{1/2}\left(\frac{P}{C^{3/2}}\right) \quad (1)$$

where K_{1C} is the fracture toughness, E the elastic modulus, H the Vickers hardness, P the load and C is the crack length.

The microhardness of the deposit cross-section was tested by a Vickers microhardness tester (BUEHLER MICROMET5104, Akashi, Japan) under a load of 300 gf for a loading time of 10 s. The elastic modulus at the direction perpendicular to the coating surface was determined through a Knoop indentation approach [17]. Knoop indentation was conducted with diamond indenter (BUEHLER MICROMET5104, Akashi, Japan) under a load of 200 gf for a loading time of 10 s. Here, the data used in Eq. (1) for the microhardness and elastic modulus of the deposits can be found in our recent report [18].

3. Results

3.1. Microstructure

To reveal the state of interlamellar bonding within the coatings prepared at different substrate temperatures, each sample was fractured along the direction perpendicular to the surface and the microstructure of the fractured surface was examined by SEM. Fig. 1 shows typical microstructures of the fractured alumina coatings. The columnar grain structure in a direction perpendicular to the lamellar plane was clearly observed in individual splats. It was evident that alumina (C1 in Fig. 1a) deposited at $240 \pm 73\ ^{\circ}C$ exhibited a lamellar structure.

However, with the increase of the substrate temperature the interlamellar bonding was improved accordingly. As the substrate temperature reached to $430 \pm 82\ ^{\circ}C$ for the sample C2, the chemical bonding recognized by long through-lamellar columnar grain was observed over a great many of lamellar interfaces (Fig. 1b). With further increase of the substrate temperature, more and more lamellar interfaces bonded chemically, as shown in Fig. 1c. In C5, most splats were bonded together. Long columnar grains were observed through the coating thickness, which means that overlaying splats were bonded as a whole. This clearly indicates continuous growth of columnar grains across splat interfaces when the surface temperature of the pre-deposited splat is greater than 430 °C for plasma-sprayed alumina coatings.

Fig. 2 shows the microstructures of the polished cross-sections for the coatings prepared at different substrate temperatures. It is clear that the lamellar structure cannot be observed for all samples even though the alumina coatings, especially for the coatings deposited at low substrate temperature (see C1 in Fig. 2a), should be composed of lamellae. This is due to the limitation of the direct observation of the coating microstructure using microscopy [19]. Large voids are visible (Fig. 2a and b). It is believed that most of these voids result from the removal of the ceramic particles during the polishing process owing to the poor intersplat bonding [3]. On the other hand, few large voids present on the cross sections of C3–C5, as shown in Fig. 2c–e. This fact suggests the formation of the improved intersplat bonding within the alumina coatings of C3–C5 deposited at high substrate temperatures. This is because a better interface bonding can prevent the well bonded splats from removal. Such fact is consistent with the bonding conditions of the alumina coatings observed from the fractured cross sections. As a result, these coatings exhibit a relatively dense microstructure.

The apparent porosity levels of the alumina coatings prepared at different substrate temperatures were determined by image analyzing using the polished cross-sectional photographs. The results (see Fig. 3) show that the apparent porosity decreases with the increase of the substrate temperature. As the substrate temperature increases from 240 to 1120 °C, the mean apparent porosity of the coatings decreases from about 17.1% to about 7.6%.

3.2. Phase structure

Fig. 4 shows the XRD patterns for both the as-received powder and the alumina coatings. It is clear that the powder is mainly comprised of α-Al_2O_3 phase. In respect of C1 and C2, due to rapid solidification of the alumina splats during spraying, the coatings consist predominantly of γ-Al_2O_3 phase. This is consistent with the results of previous reports [11,20–22]. As for C3–C5, δ-Al_2O_3 and α-Al_2O_3 become predominant phases.

To calculate the content of α-Al_2O_3 phase in the coatings, semi-quantitative analysis was carried out by following equations, for C1 and C2,

$$C_{\alpha} = \frac{I(1\,0\,4) + I(1\,1\,3) + I(1\,1\,6)}{I(1\,0\,4)+I(1\,1\,3)+I(1\,1\,6)+I(3\,1\,1)+I(4\,0\,0)+I(4\,4\,0)} \quad (2)$$

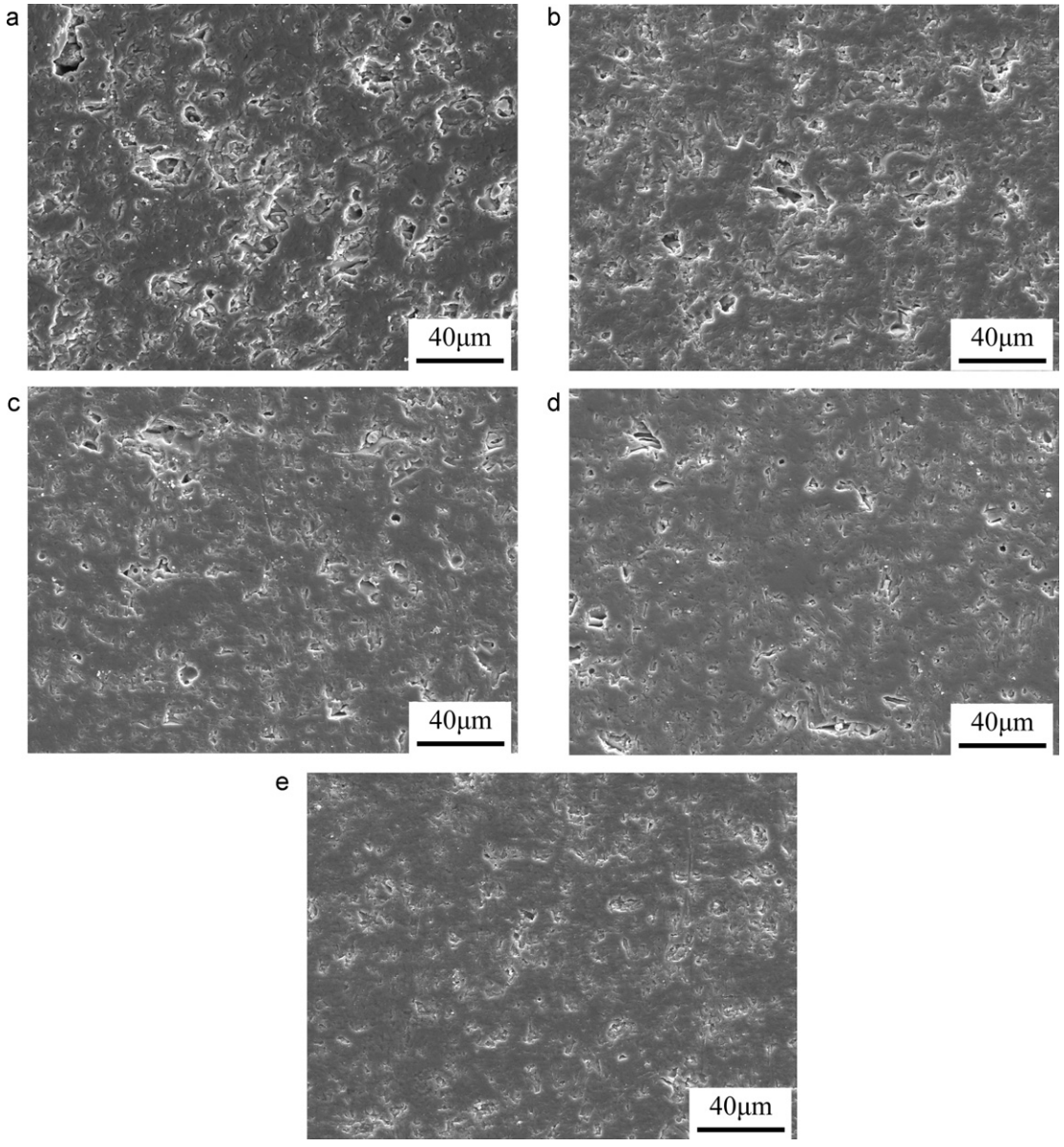

Fig. 2. Polished cross-sections for (a) C1, (b) C2, (c) C3, (d) C4, and (e) C5.

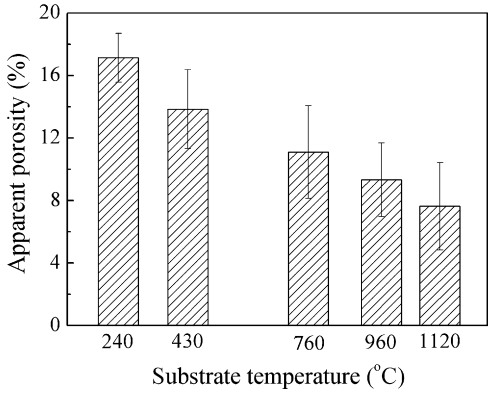

Fig. 3. The variation of apparent porosity of alumina coatings with the substrate temperature.

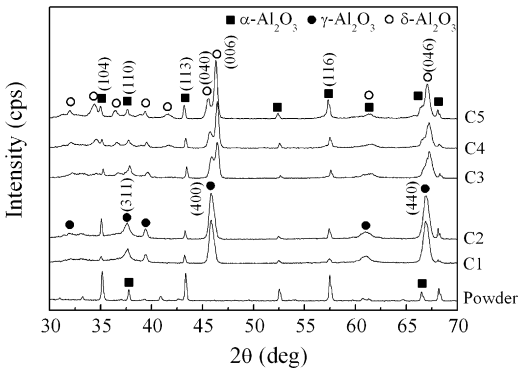

Fig. 4. Phase constituent of the alumina coatings deposited at different substrate temperatures.

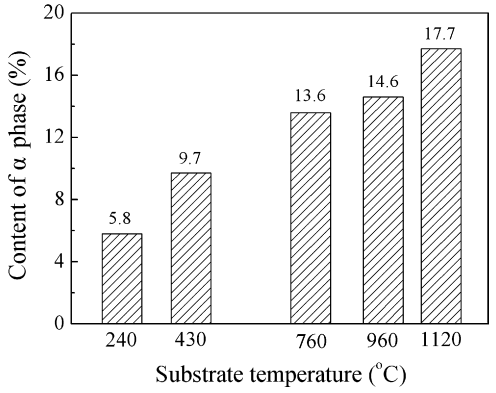

Fig. 5. Relative content of α-Al_2O_3 in the alumina coatings deposited at different substrate temperatures.

for C3, C4, and C5,

$$C_\alpha = \frac{I(1\,1\,0) + I(1\,1\,3) + I(1\,1\,6)}{I(1\,1\,0)+I(1\,1\,3)+I(1\,1\,6)+I(0\,4\,0)+I(0\,0\,6)+I(0\,4\,6)} \quad (3)$$

where C_α represents the content of α-Al_2O_3, I the area of the peak.

Fig. 5 shows the relative content of α-Al_2O_3 phase calculated by above equations for the coatings. It is found that an increase in the content of α-Al_2O_3 phase from 5.8% for C1 to 17.7% for C5 appears. It was reported that α-Al_2O_3 phase in the coatings deposited at low substrate temperature was mainly derived from unmelted particles during spraying [1,22,23]. With the increase of the substrate temperature, γ-Al_2O_3 to α-Al_2O_3 phase transformation become possible due to the high substrate temperature which provides heat treatment effect to the splats during deposition [11,20,22].

3.3. Fracture toughness

Fig. 6 shows the influence of the substrate temperature on the fracture toughness of the alumina coatings. The results clearly indicate that the fracture toughness of the alumina coatings is significantly influenced by the substrate temperature. With the coatings prepared at 240 °C, the measurement of the fracture toughness yielded a value of 1.0 ± 0.2 MPa $m^{1/2}$. However, with increasing the substrate temperature to 430 °C, the fracture toughness of the alumina coatings reached a maximum value of 2.3 ± 0.2 MPa $m^{1/2}$, which is about 69% of that for sintered bulk materials reported by Bocanegra-Bernal et al. [24] and Kim et al. [25]. As the substrate temperature increased to 1120 °C, the fracture toughness of the alumina coatings decreased to 0.6 ± 0.1 MPa $m^{1/2}$.

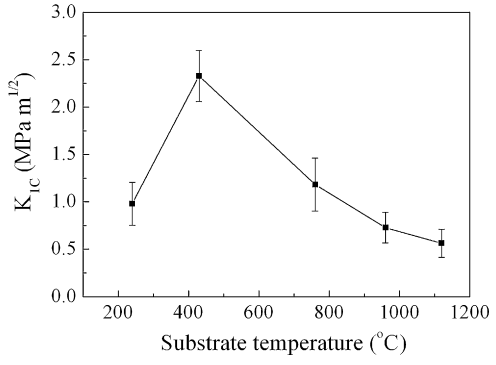

Fig. 6. Fracture toughness of the alumina coatings deposited at different substrate temperatures.

4. Discussion

4.1. The mean bonding ratio of the coatings

The present results clearly revealed that with increasing the substrate temperature (coating surface temperature) the lamellar interface bonding was significantly improved. Such increase should be mainly attributed to the epitaxial columnar grain growth across lamellar interfaces at an elevated substrate temperature. Furthermore, such significant increase in the bonding of the coatings directly resulted in the significant change of coating properties. The measurement of the mechanical properties of alumina coatings deposited at different substrate temperatures clearly revealed that the elastic modulus increased with the increase of the substrate temperature. Such increases should be attributed to the increase of the lamellar interface bonding.

According to Section 3.1, the intersplat bonding of the alumina coatings was improved by increasing the substrate temperature, especially, when the substrate temperature was above 430 °C, a rapid improvement in the intersplat bonding of the alumina coatings was found. This phenomenon can be explained by the occurrence of intersplat chemical bonding at high substrate temperatures (above 430 °C).

According to previous study [26], when the lamellar bonding ratio is less than 40%, the relative elastic modulus of thermally sprayed deposit can be expressed as follows:

$$\frac{E_c}{E} = \alpha\left[1 + 2\pi\left(\frac{a}{\delta}\right)^4 \beta^2 f(\beta)\right]^{-1} \quad (4)$$

where E_c and E are the through-thickness elastic modulus of the coating and coating materials, respectively; a is the radius of bonded area; $\beta = (\pi/8\alpha)^{0.5}$; and $f(\beta)$ is a function of β, i.e., a function of the lamellar bonding ratio α. When α becomes larger than 40%, the bending effect of the lamella during transfer of load on the additional deformation can be neglected and the above equation then is reduced to $E_c/E = \alpha$. Therefore, the mean bonding ratio of the alumina coatings can be estimated. The elastic modulus of completely dense α-Al_2O_3 and γ-Al_2O_3 is 400 and 241 GPa [26], respectively. Considering the α- and γ-phase were the main phases in all coatings and the contents of α-phase shown in Fig. 6, the elastic modulus of the coating material and the mean bonding ratio of each coating can be estimated, as shown in Table 2. Clearly, the mean bonding ratio increased from 44% to 89% with increasing the mean substrate temperature from 240 to 1120 °C.

Table 2
Mean bonding ratio of each coating estimated by the relationship between elastic modulus and the bonding ratio of the coatings.

	C1	C2	C3	C4	C5
E_c (GPa) [18]	111	141	199	231	239
E (GPa)	250	256	263	264	269
α (%)	44	55	76	88	89

4.2. The variation in the fracture toughness of the coatings

As a tensile stress occurs within the coating, cracks will propagate along the lamellar interface from the nonbonded interfaces, acting as pre-cracks. With the increase of the substrate temperature, the through-thickness columnar grains growth occurs in the coatings and the bonding ratio increases accordingly [4,5]. Crack deflection and bridging, resulting from existence of the long columnar grains in the coatings, contributes to hindering the propagation of the cracks and leads to the increase of the toughness [27–29]. This correlates directly with the change in the fracture toughness of the alumina coatings. As reported in our study [30], the fracture toughness of the YSZ (with 8 mol% Y_2O_3) coatings increases with the substrate temperature due to the improvement in the intersplat bonding. Similarly, the fracture toughness of the alumina coatings should increase with the substrate temperature. However, there exists a sharp decrease in the curve of the fracture toughness with the substrate temperature (see Fig. 6). With C3–C5, the high substrate temperature during deposition took effect as the heat treatment, which facilitated the γ-Al_2O_3 to α-Al_2O_3 phase transformation (see Figs. 4 and 5). As a transition phase for γ-Al_2O_3 to α-Al_2O_3 phase transformation, δ-Al_2O_3 phase occurs in C3–C5. According to Damani and Lutz [31], the formation of δ-Al_2O_3 in a plasma spraying process is due to a low splat cooling rate. In the case of C3–C5, with increasing the substrate temperature, the cooling rate of the splats is decreased to be around 3 °C/s, resulting in the formation of δ-Al_2O_3 phase and the change of the residual stresses. At the same time, the thermal treatment effect at high temperatures contributes to the alumina transformations under this condition. Damani and Makroczy [20] suggest that the γ-Al_2O_3 transforms continuously via the short range diffusion and re-ordering of vacancies and cations to δ-Al_2O_3 and both phases share the same lattice to some extent. This demonstrates the phase transformation from γ-Al_2O_3 to δ-Al_2O_3 can hardly induce stress. Due to high density of α-Al_2O_3, the γ-Al_2O_3 to α-Al_2O_3 phase transformation will result in volume contraction and resultant tensile stress within the coatings. Moreover, there also exists tensile thermal stress during deposition. Both the tensile stresses lead to the cracking and the further propagation of the cracks during indentation process, as shown in Fig. 7. Therefore, the significant decrease in the fracture toughness of the coatings from C2 to C5 appeared despite the existence of the long columnar grains within the coatings.

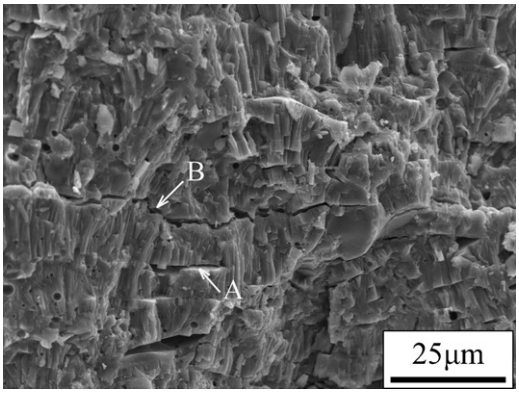

Fig. 7. SEM micrograph of the fractured cross-section of C5 shows two cracks: one is smooth nonbonded intersplat interface (marked by arrow A), the other is step-like crack (marked by arrow B) resulting from the stresses relaxation.

5. Conclusions

Alumina coatings were prepared by atmospheric plasma spraying through controlling the substrate temperature during spraying. Both the polished and fractured cross-section microstructures of the coatings were characterized by SEM. The phase structures of the coatings and the feedstock were analyzed by XRD. The changes in the microstructure and the phase structure of the alumina coatings prepared at different substrate temperatures were examined. The results show that the interlamellar bonding in the coatings is significantly improved with increasing the substrate temperature due to the continuous growth of the grains from the substrate surface. The enhancement in the bonding ratio results in an increase in the fracture toughness of the alumina coatings. However, with the stresses resulting from the thermal shrinkage and the phase transform at high substrate temperatures, the fracture toughness of the alumina coatings decreases from 2.3 ± 0.2 MPa $m^{1/2}$ to 0.6 ± 0.1 MPa $m^{1/2}$ as the substrate temperature increases from 430 to 1120 °C.

References

[1] R. McPherson, A review of microstructure and properties of plasma sprayed ceramic coatings, Surf. Coat. Technol. 39–40 (1989) 173–181.
[2] C.-J. Li, A. Ohmori, Relationships between the microstructure and properties of thermally sprayed deposits, J. Therm. Spray Technol. 11 (2002) 365–374.
[3] A. Ohmori, C.-J. Li, Quantitative characterization of the structure of plasma sprayed Al_2O_3 coating by using copper electroplating, Thin Solid Films 201 (1991) 241–252.
[4] Y.-Z. Xing, C.-J. Li, C.-X. Li, G.-J. Yang, Influence of through-lamella grain growth on ionic conductivity of plasma-sprayed yttria stabilized zirconia as an electrolyte in solid oxide fuel cells, J. Power Sources 176 (2008) 31–38.
[5] Y.-Z. Xing, C.-J. Li, Q. Zhang, C.-X. Li, G.-J. Yang, Influence of microstructure on the ionic conductivity of plasma-sprayed yttria-stabilized zirconia deposits, J. Am. Ceram. Soc. 91 (2008) 3931–3936.
[6] A. Tricoire, M. Vardelle, P. Fauchais, F. Braillard, A. Malié, P. Bengtsson, Macrocrack formation in plasma-sprayed YSZ TBCs when spraying thick passes, High Temp. Mater. Process. 9 (2005) 401–413.
[7] I.-H. Jung, K.-K. Bae, M.-S. Yang, S.-K. Ihm, A study of the microstructure of yttria-stabilized zirconia deposited by inductively coupled plasma spraying, J. Therm. Spray Technol. 9 (2000) 463–477.

[8] I.-H. Jung, J.-S. Moon, K.-C. Song, M.-S. Yang, Microstructure of yttria stabilized zirconia deposited by plasma spraying, Surf. Coat. Technol. 180–181 (2004) 454–457.
[9] H.B. Guo, R. Vaβen, D. Stöver, Atmospheric plasma sprayed thick thermal barrier coatings with high segmentation crack density, Surf. Coat. Technol. 186 (2004) 353–363.
[10] H.B. Guo, S. Kuroda, H. Murakami, Microstructures and properties of plasma-spayed segmented thermal barrier coatings, J. Am. Ceram. Soc. 89 (2006) 1432–1439.
[11] G.N. Heintze, S. Uematsu, Preparation and structures of plasma-sprayed γ- and α-Al_2O_3 coatings, Surf. Coat. Technol. 50 (1992) 213–222.
[12] G.R. Anstis, P. Chantikul, B.R. Lawn, D.B. Marshall, A critical evaluation of indentation techniques for measuring fracture toughness: I. Direct crack measurements, J. Am. Ceram. Soc. 64 (1981) 533–538.
[13] K. Niihara, A fracture mechanics analysis of indentation-induced Palmqvist crack in ceramics, J. Mater. Sci. Lett. 2 (1983) 221–223.
[14] M.M. Lima, C. Godoy, J.C. Avelar-Batista, P.J. Modenesi, Toughness evaluation of HVOF WC-Co coatings using non-linear regression analysis, Mater. Sci. Eng. A 357 (2003) 337–345.
[15] A. Jadhav, N.P. Padture, F. Wu, E.H. Jordan, M. Gell, Thick ceramic thermal barrier coatings with high durability deposited using solution-precursor plasma spray, Mater. Sci. Eng. A 405 (2005) 313–320.
[16] Y. Li, K.A. Khor, Mechanical properties of the plasma-sprayed Al_2O_3/$ZrSiO_4$coatings, Surf. Coat. Technol. 150 (2002) 143–150.
[17] D.B. Marshall, T. Noma, A.G. Evans, A simple method for determining elastic-modulus-to-hardness ratios using Knoop indentation measurements, J. Am. Ceram. Soc. 65 (1982) C175–C176.
[18] Y.-Z. Xing, C.-P. Jiang, H. Chen, J.-M. Hao, Microstructure and mechanical properties of alumina coatings plasma-sprayed at different substrate temperatures, Acta Mech. Solida Sin. 24 (2011) 461–466.
[19] C.-J. Li, W.-Z. Wang, Quantitative characterization of lamellar microstructure of plasma-sprayed ceramic coatings through visualization of void distribution, Mater. Sci. Eng. A 386 (2004) 10–19.
[20] R.J. Damani, P. Makroczy, Heat treatment induced phase and microstructural development in bulk plasma sprayed alumina, J. Eur. Ceram. Soc. 20 (2000) 867–888.
[21] A. Kulkarni, J. Gutleber, S. Sampath, A. Goland, W.B. Lindquist, H. Herman, A.J. Allen, B. Dowd, Studies of the microstructure and properties of dense ceramic coatings produced by high-velocity oxygen-fuel combustion spraying, Mater. Sci. Eng. A 369 (2004) 124–137.
[22] C.C. Stahr, S. Saaro, L.-M. Berger, J. Dubsky, K. Neufuss, M. Herrmann, Dependence of the stabilization of α-alumina on the spray process, J. Therm. Spray Technol. 16 (2007) 822–830.
[23] R. McPherson, On the formation of thermally sprayed alumina coatings, J. Mater. Sci. 15 (1980) 3141–3149.
[24] M.H. Bocanegra-Bernal, C. Domínguez-Rios, A. Garcia-Reyes, A. Aguilar-Elguezabal, J. Echeberria, A. Nevarez-Rascon, Fracture toughness of an α-Al_2O_3 ceramic for joint prostheses under sinter and sinter-HIP conditions, Int. J. Refract. Met. Hard Mater. 27 (2009) 722–728.
[25] S.W. Kim, W.S. Chung, K.-S. Sohn, C.-Y. Son, S. Lee, Improvement of flexure strength and fracture toughness in alumina matrix composites reinforced with carbon nanotubes, Mater. Sci. Eng. A 517 (2009) 293–299.
[26] C.-J. Li, A. Ohmori, R. McPherson, The relationship between microstructure and Young's modulus of thermally sprayed ceramic coatings, J. Mater. Sci. 32 (1997) 997–1004.
[27] C.W. Li, J. Yamanis, Super-tough silicon nitride with R-curve behavior, Ceram. Eng. Sci. Proc. 10 (1989) 632–645.
[28] P.F. Becher, Microstructural design of toughened ceramics, J. Am. Ceram. Soc. 74 (1991) 255–269.
[29] Z. Xie, L. Gao, W. Li, L. Xu, X. Wang, High toughness alumina ceramics with elongated grains developed from seeds, Sci. China Ser. E 46 (2003) 527–536.
[30] Y.-Z. Xing, C.-J. Li, C.-X. Li, G.-J. Yang, Relationship between the interlamellar bonding and properties of plasma sprayed Y_2O_3–ZrO_2 coatings, in: B.R. Marple, M.M. Hyland, Y.-C. Lau, C.-J. Li, R.S. Lima, G. Montavon (Eds.), Thermal Spray 2009: Proceedings of the International Thermal Spray Conference, Las Vegas, May 4–7, (2009), pp. 939–944.
[31] R.J. Damani, E.H. Lutz, Microstructure, strength and fracture characteristics of a free-standing plasma-sprayed alumina, J. Eur. Ceram. Soc. 17 (1997) 1351–1359.